JOURNAL OF MATERIALS SCIENCE **39** (2004) 7207–7212

Simulation of equiaxed growth ahead of an advancing columnar front in directionally solidified Ni-based superalloys

H. B. DONG, X. L. YANG, P. D. LEE
Department of Materials, Imperial College London, London SW7 2BP, UK
E-mail: p.d.lee@imperial.ac.uk

W. WANG
Alcoa Technical Center, 100 Technical Drive, Alcoa Center, PA 15069, USA

Growth of equiaxed grains ahead of an advancing columnar front leads to the formation of as-cast defects, such as stray grains in single crystals or tree rings in vacuum arc remelting (VAR) ingots. In this study a combined cellular automata-finite difference model was applied to simulate dendrite growth and the formation of equiaxed grains in directionally solidified nickel-based superalloys. Realistic dendritic structures and complex solute concentration profiles at the growth front were simulated. It was observed that the solute interaction between primary dendrites occurs well below their tips, while strong solute interaction occurs between the diffusion fields of secondary and tertiary arms. The influence of thermal gradient and growth velocity on CET was investigated and the results were combined on a CET map, showing that a decrease in thermal gradient and an increase in growth rate favour a CET.

1. Introduction

In directionally solidified or single crystal (SX) superalloys, columnar grains are desirable, with equiaxed grains being treated as casting defects since high angle boundaries must be avoided [1]. To achieve a columnar dendritic structure, high temperature gradients in front of the solid/liquid interface and low solidification velocities are used to prevent the columnar-to-equiaxed transition (CET), thus eliminating the formation of stray grains [2]. In secondary remelting processes, such as vacuum arc remelting (VAR), perturbations in the process parameters can lead to the formation of strings of equiaxed grains ahead of the columnar front. The strings of equiaxed grains are usually termed "tree rings" and may be linked to detrimental defects such as freckles [3]. To understand the formation of equiaxed grains ahead of columnar dendrites, a fundamental knowledge of the CET is required.

Factors affecting CET have been reviewed by Hunt [4] and the first analytical model of CET was developed by him, based on equiaxed grains nucleated in the constitutionally undercooled region ahead of the columnar growth front. The influences of alloy composition, temperature gradient ahead of the growth front, and tip growth rate on CET were revealed. Hunt's model was modified by Gaumann, Trivedi and Kurz [5] by updating the analytical dendritic growth model, increasing the accuracy of the calculation of dendrite tip undercooling by inclusion of non-equilibrium effects. The above models use a simplified geometry for the growth of solid phases and are deterministic models; they can only predict the average growth of the phases rather than the distribution of sizes. Recently, coupled cellular automaton with finite element (CA-FE) probabilistic models have been used to predict the solidification structures and to simulate the CET [6]. Compared with analytical models, the advantages of the probabilistic CA-FE model are that the individual grains are identified, and their shapes and sizes can be shown graphically during solidification. However, the CA-FE model is based on the assumption that the envelope of the growing grains can be approximated as isolated primary dendrite tips, allowing the analytical solution of Kurz, Giovanola and Trivedi [7] (the KGT model) to be applied. By using the KGT model to relate thermal undercooling to the restriction in grain growth due to solute built-up ahead of ideal dendrite tips, the CA-FE model only requires the thermal field to be solved, not the solute field. Therefore the CA-FE model cannot be used to simulate the dendrite structure and the solute interactions at the growth front and hence the constitutional undercooling, which is critical to determine the nucleation ahead of the columnar front [8, 9].

In this study a coupled cellular automata-finite difference (CA-FD) model is applied to simulate the dendritic growth and to predict the CET in directionally solidified nickel based superalloys. The CA-FD is an extension of the cellular automata technique to include solute diffusion through combination with a finite difference solver. This extension was first used

to simulate the solidification structure by Spittle [10] using a stepped front motion technique. In his model the status of an individual cell can either be solid or liquid. Nastac [11] and Lee [12] coupled a more accurate front tracking technique with solid fraction evolution in each growing cell, and their models allow the resolution of not only the grain envelopes but also the dendritic structures. The model used in this study is based on the approach of Lee *et al*. [12], and crystallographic anisotropy of cubic metals is accounted for by an adapted decentred square growth algorithm [13, 14].

The aim of this work is to present the simulated results of the growth of equiaxed grains ahead of an advancing columnar front in directionally solidified Ni-based superalloys using a coupled cellular automata-finite difference model. It is the first to simulate the CET with detailed dendritic structures, which can be shown graphically during transition. In this paper, a brief description of the CA-FD model is presented first, then simulated results on dendritic evolution and columnar-to-equiaxed transition are reported and finally the influences of process variables (thermal gradient and growth rate) on the columnar-to-equiaxed transition are discussed.

2. Model theory

The present model combines a cellular automaton description of grain growth with a finite difference solver for solute diffusion. Details of the model are given in references [12, 14–17]. The model is, therefore, only briefly summarised here.

2.1. Model description

Both the CA and FD components of the model run on the same regular spatial square grid and the same time step. Each spatial cell can exist in three states: liquid, solid or growing (i.e., a mixture of solid and liquid). The model starts with all cells in a liquid state, and the cells transform to the growing state either by a nucleation event or due to growth proceeding from a neighbouring cell. In a growing cell, local equilibrium is assumed at the solid/liquid interface and the solute is partitioned between the solid and liquid phases. The change in the solute concentration and the curvature of the interface affects the degree of undercooling and hence feeds back to the nucleation and growth process during each time step of calculation.

Nucleation for equiaxed grains is determined stochastically to represent the essentially random process of nucleation in bulk liquid. Nucleation at the bottom surface of the domain is fixed prior to the calculation with one of its ⟨100⟩ crystallographic direction aligned with the vertical temperature gradient. In a growing cell, once the change in solid fraction is obtained by explicitly solving the solute diffusion equations, the growth algorithm of the solid is governed by an adapted decentred square method to account for the effect of crystallographic anisotropy [14].

TABLE I Properties of the binary approximation of a Ni-based superalloy

Parameter	Variable	Value
Liquidus temperature	T_L	1658 K
Solidus temperature	T_S	1593 K
Liquidus slope	m	−10.9 K/wt%
Partition coefficient	k	0.48
Diffusion coefficient in liquid	D_L	3.0×10^{-9} m^2/s
Diffusion coefficient in solid	D_S	3.0×10^{-12} m^2/s
Gibbs Thomson coefficient	Γ	1.0×10^{-7} K·m
Initial concentration	C_0	4.85 wt%

2.2. Simulation parameters

Simulations were performed on a regular square grid in 2D with a cell edge length of 5 μm. The size of the domain was 2.5 mm wide by 4 mm high with a total number of 500 × 800 cells in the domain. The time step was 1 ms. A zero flux boundary condition was applied to the left and right sides of the domain, and a positive temperature gradient was imposed, moving from the bottom to the top in the domain to simulate the thermal profile during directional solidification. A binary approximation of a nickel-based superalloy was used in this simulation. The actual alloy composition is complex, therefore, the element with the lowest diffusion coefficient (D_L), high content and partition coefficient (k) farthest from unity is considered. The material properties used in the simulation are given in Table I.

Most commercial Ni-based superalloys contain more than five elements and the equilibrium partition ratios usually are not constant due to the solute interaction. Sung and Poirier [18] reviewed the liquid-solid partition ratios in nickel-based alloys. The measured partition coefficients of Nb in Nickel based superalloys range from 0.24 to 0.50 around the liquidus temperatures. Recently Yang *et al*. [19] experimentally observed the partition coefficient of Nb increases with fraction solid evolution in superalloys. However there is still a paucity of detailed data of partition coefficient for multi-component superalloys. In this study a constant value of 0.48 was used [20].

3. Results and discussion

In this section, simulated results on the evolution of dendritic structures and formation of equiaxed grains ahead of advancing columnar dendrites are reported. The solute concentration ahead of the growth front is then presented, and finally the influence of process variables on the columnar-to-equiaxed transition is discussed.

3.1. Evolution of dendritic structures and formation of equiaxed grains in CA-FD simulations

A typical dendrite structure produced by the simulation is shown in Fig. 1a. This figure shows the predicted transition from a columnar structure to an equiaxed one. The conditions were: an imposed vertical temperate gradient (G) of 10 K/mm; pulling velocity (V) varied as a function of simulation time (t): $V = 30 + 4 \times t$

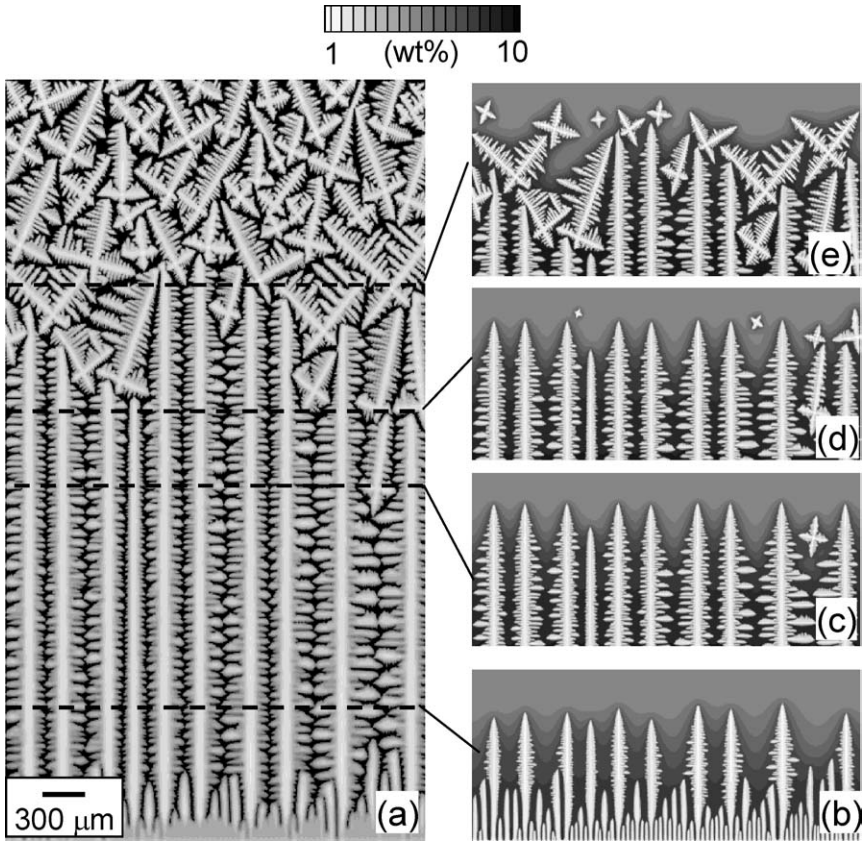

Figure 1 Simulated dendritic structures of the binary approximation showing the microstructure features and the columnar to equiaxed transition: (a) the whole dendritic structure at $t = 40$ s and the solidification front at different times of (b) $t = 15$ s, (c) $t = 25$ s, (d) $t = 27$ s and (e) $t = 30$ s.

(μm/s); nucleation undercooling (ΔT_N) was approximated from DTA measurements [21], and a mean nucleation undercooling of 14 K with a standard deviation of 1 K was used in the simulation; maximum nucleation density was set to $6.0 \times 10^{12} m^{-3}$. As shown in Fig. 1b, solidification started from the bottom and a thin layer of fine grains grew from prefixed seeds. Among the many grains formed at the bottom surface of the ingot, only a few long columnar grains succeeded in growing. The competitive growth occurring among columnar grains is shown in Fig. 1b, c and d. Primary columnar dendrites grew from the bottom, secondary dendritic arms developed from the primary stems, and some tertiary dendritic arms started to initiate from secondary arms. For metals with a cubic structure, these primary dendrites have a favourable orientation with one of its ⟨100⟩ directions aligned with the vertical heat flow. It should be pointed out that the simulated primary dendrite arm spacing is not uniform as assumed in deterministic models. The predicted maximum spacing is 430 μm and the minimum spacing is 170 μm. The simulated primary spacings have a similar range to those observed experimentally [22]. However the predicted upper and lower limits in spacing are higher than experimental results. This discrepancy may be due to the experiments being carried out in 3D and the simulation in 2D.

As shown in Fig 1c and d, in the columnar region, a few grains nucleated in the bulk liquid between the primary dendrites, but the structure is still dominated by columnar dendrites. Those nucleated grains often do not have a favourable orientation with respect to the vertical heat flow; therefore they are overgrown by the selected columnar grains and appear as small "islands" in the columnar dendritic region. In practice those nucleated grains in DS and SX castings are acceptable if their volume fraction is small. As solidification continues, the pulling rate increases and the undercooled region ahead of the columnar tips becomes bigger, which favours the nucleation ahead of the columnar dendritic tip. At $t = 30$ s, the nucleated grains finally block the columnar front as shown in Fig. 1e, where columnar-to-equiaxed transition occurs. The nucleated grains immediately ahead of the columnar grains, however, still have a relatively elongated shape due to the imposed vertical thermal gradient. These grains will become truly equiaxed when the thermal gradient in the solidifying region approaches zero or a sudden change (perturbation) occurs, as observed in VAR. For an example, Fig. 2 shows strings of equiaxed grains formed between the dendrites in the columnar region of VAR ingots due to velocity perturbation [3].

In summary, the CET was clearly simulated by the CA-FD model showing detailed grain structures and dendritic features. The grains grown immediately ahead of the columnar dendrites tend to be elongated along the pulling direction, and the CET is a gradual transition.

3.2. Solute concentration profiles

The CA-FD is a solute diffusion controlled solidification model. The change in the solute concentration affects the degree of undercooling and hence feeds back to the nucleation and growth processes during each time

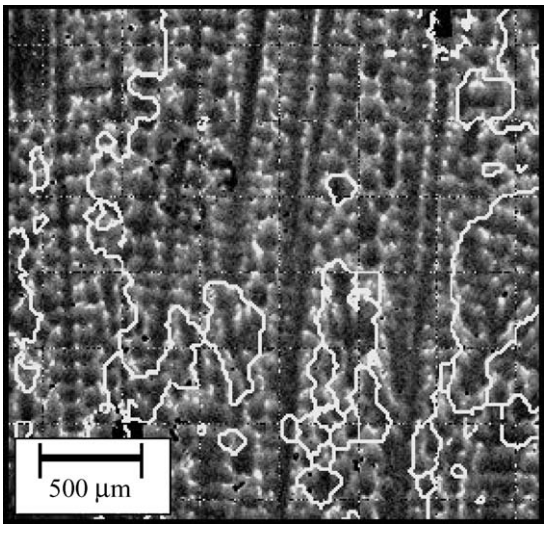

Figure 2 Dendritic structures and the CET shown by backscattered SEM overlaid with the grain boundaries mapped by EBSD. (After reference [3]).

step of calculation. In this section the calculated solute concentration profile ahead of the growth front is presented and solute interaction ahead of growth front is discussed.

Fig. 3 shows a contour map of simulated solute concentration and solute analysis along the lines perpendicular to the pulling direction. As shown in Fig. 3a, the contour plot reveals that composition profiles ahead of the array of columnar dendrites do not have a similar form, and concentration profiles strongly depend on the spacing of the dendrites. If dendritic tips are close, as shown in the region A in the figure, dendrites interact with each other through solute diffusion interaction near their tips. One of them might be overgrown by its neighbouring dendrites. If two dendritic tips are far apart, as shown in region B of the figure, the two dendrites cannot interact with one another at the tip and dendritic branching may occur if tertiary arms can block off secondary arms. This is a competitive growth problem which depends on the interaction between diffusion fields of the secondary and tertiary tips.

Detailed concentration profiles along the lines perpendicular to the pulling direction are shown in Fig. 3b and c. The line I-I is taken near the dendritic columnar front and the line II-II is taken far away from the columnar front. As shown in the line I-I, solute concentration around the tip is higher than the concentration between dendrites, so a solute gradient perpendicular to pulling direction exists between the columnar dendrite tips. This observed phenomenon agrees with Burden and Hunt's analytical model [23]. In their analysis a radial solute gradient around the tip is added to the composition gradient ahead of the tip in order to take away the rejected solute. Fig. 3b shows that the composition between most dendrite tips is at the bulk liquid level. This means that the two columnar dendrites do not interact with one another at their tips and the growth of primary dendrites at the tip at this stage can be treated in isolation. Calculated concentration profiles at a later stage of solidification are shown in Fig. 3c. This line shows that the solute concentration perpendicular to the pulling direction is nearly uniform, and its exponential profile from the interface to the bulk liquid is hard to see. This means that there are strong interactions among diffusion fields of secondary arms and possible tertiary arms, and secondary dendrites can not be treated in isolation. The above observations reveal that a complex diffusion profile exists in different solidification regions at different stages of solidification. This agrees well with experimental observation in the transparent succinonitrile-acetone system [24].

Fig. 4 shows concentration profiles along the lines parallel to the pulling direction crossing a dendritic core (I-I line) and within the interdendritic region between primary columnar dendrites (II-II line). The I-I line shows that at the tip of the primary dendrite the

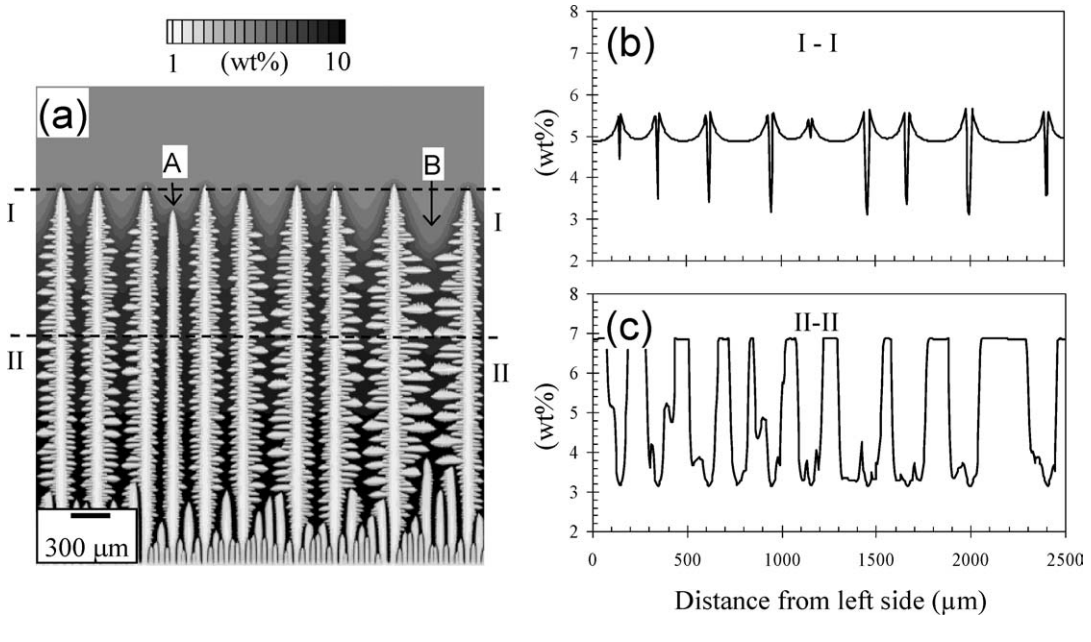

Figure 3 (a) A contour map of simulated solute concentration. (b) Solute analysis along the line (I-I) perpendicular to the pulling direction near the columnar dendritic front. (c) Solute analysis along the line (II-II) perpendicular to the pulling direction away from the columnar dendritic front.

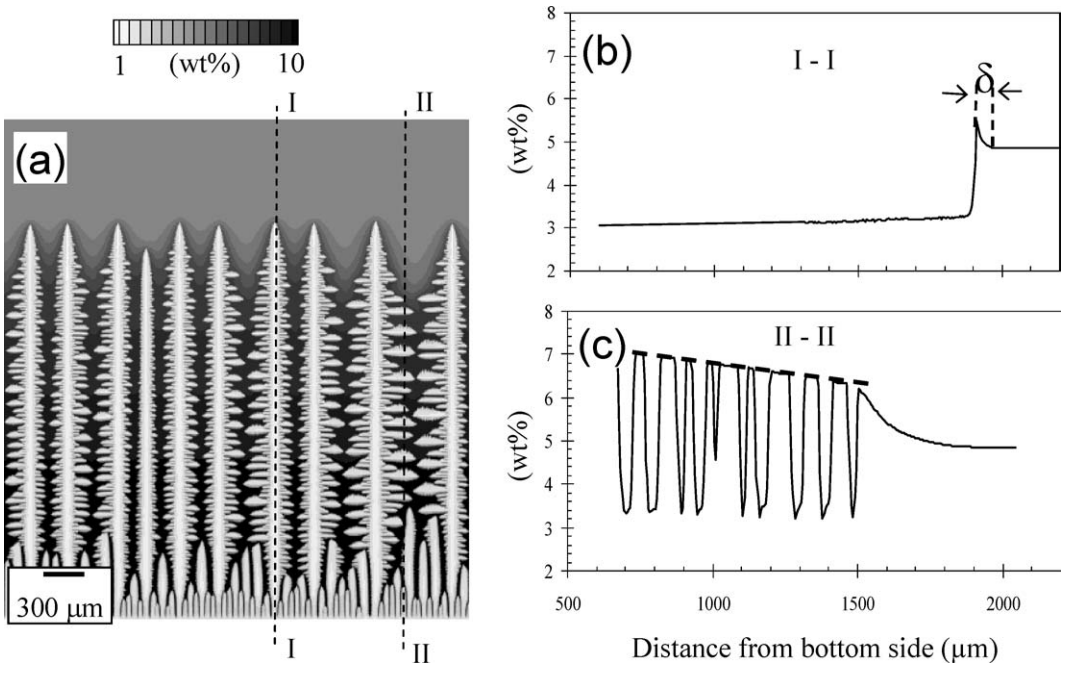

Figure 4 (a) A contour map of simulated solute concentration and (b) solute analysis along the line (I-I) parallel to the pulling direction crossing the dendritic core and (c) solute analysis along the line (II-II) parallel to the pulling direction within the interdendrtic region.

solute composition in liquid decays exponentially from its value at the interface to the bulk liquid composition, and the thickness of the diffusion layer (δ) is in the same order of the half of averaged primary dendrite arm spacing. This agrees with EPMA results for solute analysis ahead of a dendritic growth front [25]. A gradual increase in solute concentration is also observed in the line I-I from the bottom to the tip. This gradual increase is due to an increased pulling velocity applied in the simulation. Since equilibrium is assumed at the interface and a straight solidus line is used in the calculation, an increase in tip undercooling will give an increase in solute concentration.

The II-II line shows a solute profile within the interdendritic region between primary columnar dendrites. When the II-II line crosses solid phases, the solute concentration is at a lower level; when it crosses the liquid region, the solute concentration is at a higher level, and a solute gradient is observed from the bottom to the top in the liquid region. A line is fitted to the solute concentrations in the liquid regions and gives a slope of -0.97×10^{-3} wt%/μm. Ignoring any local curvature of the interface, the concentration gradient in liquid regions along the line II-II can be modelled analytically following reference [23] as: $\mathrm{d}C_\mathrm{L}/\mathrm{d}x = G/m$, where G is the temperature gradient and m is the slope of the liquidus line. Substituting the actual value in the equation gives: $\mathrm{d}C_\mathrm{L}/\mathrm{d}x = -1.0 \times 10^{-3}$. This agrees well with the simulated value.

Although there may be inaccuracies in the solute diffusion calculation due to the large cell size and 2-D simplification, the relative diffusion profile is shown to be correct. It can be concluded that the present CA-FD model can produce realistic dendritic structures and complex solute concentration profiles at the growth front. For primary dendrites, solute interaction is well below the tips, but strong interaction occurs among diffusion fields of secondary arms and possible tertiary arms at the later stage of solidification. The liquid between the dendrites has sufficient time to become homogenous perpendicular to the pulling direction. The composition gradient along the pulling direction in the liquid between dendrites can be approximated by the ratio of thermal gradient to the slope of the liquidus line.

3.3. The influence of processing variables on the CET

Simulations were carried out to investigate the influence of growth velocity and thermal gradient on the CET. Results and discussion are presented in this section. Since the CET is a gradual transition with intermediate stages, it is difficult to give a precise CET criterion. In this study, for the purpose of simplification, the CET occurs if more than half of the columnar dendritic fronts are blocked by equiaxed grains.

Fig. 5 shows a map in which the CET is plotted as a function of temperature gradient and growth velocity

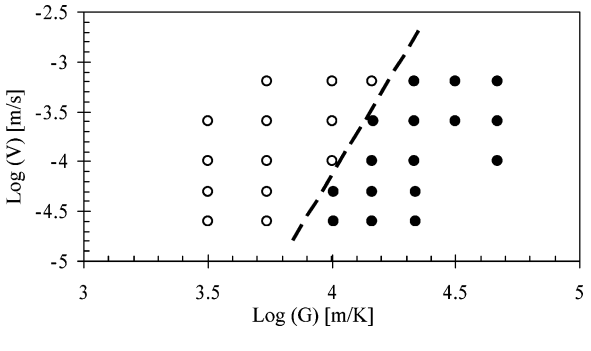

Figure 5 A CET map showing the influences of the temperature gradient and growth velocity on the CET. The open and filled circles indicate the equiaxed and columnar grains respectively. The dashed line separates the equiaxed and columnar regions.

using a mean nucleation undercooling of 14 K and a maximum nucleation density of $6.0 \times 10^{12}\mathrm{m}^{-3}$. Filled and open circles indicate columnar grains and equiaxed grains, respectively. The dashed line is an approximate CET line which separates the equiaxed and columnar regions.

As shown in Fig. 5, at a given temperature gradient, an increase in growth velocity leads to CET. This is because an increase in growth velocity will increase solute concentration ahead of the dendrite tip. As an example, for a temperature gradient of 10 K/mm, solute concentration immediately ahead of a columnar dendritic tip is simulated as 5.41 wt% at a pulling velocity of 90 μm/s, and it increases to 5.66 wt% at a pulling velocity of 134 μm/s, which gives an increase of 4.5% in solute concentration. This relationship can also be examined using an analytical model [5] $C_{\mathrm{L}}^{*} = C_0/(1 - (1 - k_{\mathrm{V}})I_v[P_{\mathrm{c}}])$, where C_{L}^{*} is the composition of the liquid at the tip, k_{V} is the velocity dependent partition coefficient, I_{v} is the Ivantsov function, P_{c} is the solutal Péclet number, which is given by: $P_{\mathrm{c}} = RV/2D$. Using a secondary approximation to the Ivantsov function and assuming a constant tip radius, a relative change in concentration of 5.1% is obtained, which agrees well with the simulated value. An increase in solute content ahead of the tip leads to an increase in tip undercooling, which favours the nucleation of equiaxed grains, leading to the columnar-to-equiaxed transition.

For a given growth velocity as shown in Fig. 5, a decrease in G favours the formation of equiaxed grains. This is because a decrease in G leads to an increase in the width and magnitude of the undercooled region ahead of the columnar front, which again promotes the nucleation of equiaxed grains and columnar-to-equiaxed transition.

The above results and analysis conclude that CA-FD simulations successfully illustrate the trend of the influence of temperature gradient and growth velocity on CET, and a decrease in thermal gradient and an increase in growth rate favour the formation of equiaxed grains.

4. Conclusions

Columnar-to-equiaxed transition was successfully simulated by the CA-FD model with dendritic features. The simulations show that the CET is a gradual transition, and that the grains grown immediately ahead of the columnar dendrites tend to be elongated along the pulling direction. Realistic dendritic structures and complex solute concentration profiles at the growth front are presented. Strong solute interaction occurs among diffusion fields of secondary and tertiary arms, but the interaction between primary dendrites is well below the tips. It was observed that at the later stage of solidification solute concentration in the liquid between the dendrites becomes homogenous along the line perpendicular to the pulling direction, and a solutal gradient along the pulling direction in the liquid can be approximated by the ratio of the thermal gradient to the slope of the liquidus line. The trends of influence of temperature gradient and pulling velocity on CET are combined on a CET map, showing that a decrease in thermal gradient and an increase in growth rate favour the columnar-to-equiaxed transition.

Acknowledgment

The authors would like to thank the EPSRC (Grant no. GR/R78992) for financial support and the industrial collaborators (Rolls-Royce plc, Cannon Muskegon and ESI software Paris) for their assistance and the provision of information.

References

1. R. E. NAPOLITANO and R. J. SCHAEFER, *J. Mater. Sci.* **35** (2000) 1641.
2. N. D'SOUZA, M. G. ARDAKANI, M. MCLEAN and B. A. SHOLLOCK, *Metall. Mater.Trans.* A **31** (2000) 2877.
3. X. XU, W. ZHANG and P. D. LEE, *ibid.* A **33** (2002) 1805.
4. J. D. HUNT, *Mater. Sci. Eng.* **65** (1984) 75.
5. M. GAUMANN, R. TRIVEDI and W. KURZ, *ibid.* A **226** (1997) 763.
6. C. A. GANDIN and M. RAPPAZ, *Acta Metall. Mater.* **42** (1994) 2233.
7. W. KURZ, B. GIOVANOLA and R. TRIVEDI, *Acta Metall.* **34** (1986) 823.
8. J. D. HUNT and S. C. FLOOD, *J. Cryst. Growth* **82** (1987) 552.
9. *Idem., ibid.* **82** (1987) 543.
10. J. A. SPITTLE and S. G. R. BROWN, *Acta Metall.* **37** (1989) 1803.
11. L. NASTAC, *Acta Mater.* **47** (1999) 4253.
12. D. SEE, R. C. ATWOOD and P. D. LEE, *J. Mater. Sci.* **36** (2001) 3423.
13. W. WANG, A. KERMANPUR, P. D. LEE and M. MCLEAN, *Int. J. Cast. Metals Res.* **15** (2002) 269.
14. W. WANG, P. D. LEE and M. MCLEAN, *Acta Mater.* **51** (2003) 2971.
15. W. WANG, A. KERMANPUR, P. D. LEE and M. MCLEAN, *J. Mater. Sci.* **38** (2003) 4385.
16. R. C. ATWOOD and P. D. LEE, *Metall. Mater.Trans.* B **33** (2002) 209.
17. P. D. LEE, R. C. ATWOOD, R. J. DASHWOOD and H. NAGAUMI, *Mater. Sci. Eng.* A **328** (2002) 213.
18. P. K. SUNG and D. R. POIRIER, *Metall. Mater.Trans.* A **30** (1999) 2173.
19. W. H. YANG, W. CHEN, K. M. CHANG, S. MANNAN and J. DEBARBADILLO, Superalloys 2000, Warrendale MINERALS METALS & MATERIALS SOC, 2000, p. 75.
20. L. NASTAC and D. M. STEFANESCU, *Metall. Mater.Trans.* A **28** (1997) 1582.
21. N. D'SOUZA, M. G. ARDAKANI, A. WAGNER, B. A. SHOLLOCK and M. MCLEAN, *J. Mater. Sci.* **37** (2002) 481.
22. A. KERMANPUR, W. WANG, P. D. LEE and M. MCLEAN, *Mater. Sci. Techn.* **19** (2003) 859.
23. BURDEN and J. D. HUNT, *J. Cryst. Growth* **22** (1974) 104.
24. X. WAN, Q. HAN and J. D. HUNT, *Acta Mater.* **45** (1997) 3975.
25. M. R. M. SHIN, DPhil thesis, University of Oxford, 2002.

Received 17 March
and accepted 29 June 2004